RSC Advances

PAPER

View Article Online
View Journal | View Issue

Cite this: *RSC Adv.*, 2017, **7**, 30411

A facile Pechini sol–gel synthesis of $TiO_2/Zn_2TiO_2/ZnO/C$ nanocomposite: an efficient catalyst for the photocatalytic degradation of Orange G textile dye

Mostafa Y. Nassar,* Ayman A. Ali and Alaa S. Amin

We have developed an efficient route for the synthesis of $TiO_2/Zn_2TiO_2/ZnO/C$ nanocomposites through a Pechini sol–gel method followed by heat treatment at 550 °C for 30 min. The produced phases and their crystallite sizes have been controlled by varying the Ti^{4+} : Zn^{2+} molar ratios. FE-SEM, FT-IR, XRD, TEM, diffuse reflectance spectroscopy (DRS) and thermal analysis techniques were utilized for characterization of the as-prepared products. The photocatalytic activity of the products was investigated. Superior activity was observed for the $TiO_2/Zn_2TiO_2/ZnO/C$ nanocomposite for the photocatalytic degradation of Orange G dye (OG) under sunlight and UV illumination with *ca.* 100% degradation in 50 and 120 min, respectively. The kinetic studies showed that the observed first-order rate constant (k_{obs}) was 113.48 × 10^{-3} and 29.46 × 10^{-3} min^{-1} for the photocatalytic degradation under sunlight and UV irradiation, respectively. The results also showed the stability and reusability of the as-prepared nanocomposite and its applicability for the removal of OG textile dye from aqueous media.

Received 1st May 2017
Accepted 8th June 2017

DOI: 10.1039/c7ra04899h

rsc.li/rsc-advances

1. Introduction

The textile industry is one of the major sources of environmental pollution due to a discharge of the textile dyes into the environment after the dyeing process without treatment.[1–3] Among these pollutants, reactive dyes (*e.g.* Orange G dye (OG)) are the most harmful dyes owing to the carcinogenicity and toxicity of the dyes because of the presence of azo groups (–N=N–) in their chemical structures.[4–6] Removal of contaminants from wastewater has become a crucial demand for humanity. Thus, many researchers have devoted much of their research work to the treatment of wastewater of the textile industries before the disposal process.[7–9] To date, different chemical, biological, and physical procedures have been proposed for the removal of pollutants from wastewater including chemical oxidation, precipitation, reverse osmosis, filtration, membrane process, solvent extraction, adsorption, electrochemical and ultrasonic technique, biological treatment, and coagulation.[6,10–15]

On the other hand, the photocatalytic degradation process has proven its efficiency for the removal of various textile dyes.[16–20] This technique depends on the generation of hydroxyl radicals due to the presence of a catalyst and light, which lead to degradation or completely mineralization of the dyes into nontoxic species, CO_2 and H_2O.[21] Among the catalysts, titanium oxide (TiO_2), especially the anatase phase, is one of the most attractive catalysts in the photocatalysis applications due to its chemical stability, inexpensiveness, non-toxicity, and good optoelectronic properties.[22] However, this semiconductor has a wide band gap which exceeds 3.2 eV. Hence, the catalytic applications of this catalyst under sunlight irradiation are limited because the TiO_2 catalyst needs ultraviolet light for its activation.[23] Besides, the high recombination rate of the electron–hole (e–h) pair is the second limitation of the TiO_2 photocatalyst.[23–25] Additionally, zinc oxide (ZnO) has received a great attention as an alternative photocatalyst owing to its non-toxicity, high catalytic efficiency, as well as low cost, and it has similar band gap energy to that of TiO_2.[26–29] However, the band gap energy of ZnO photocatalyst is still large (*ca.* 3.2 eV) so that it is only applicable under UV irradiation.[30] Thus, TiO_2 catalyst can be coupled with ZnO to enhance its photocatalytic activity through reducing the charge carrier recombination rate and enhancing its visible-light photocatalytic activity.[31–33] Because of the importance of TiO_2/ZnO nanocatalyst, some methods have been adopted to fabricate this nanocomposite such as sol–gel,[34–36] ultrasound-assisted sol–gel, atomic layer deposition,[37] microwave irradiation,[38] solid-state dispersion,[30] pulsed laser ablation,[39] and hydrothermal method.[36]

In addition, synthesis of TiO_2/ZnO nanocomposite using a facile and low-cost synthetic method is still a challenge, and the adopted procedures may require high temperatures, tedious work, and/or special equipment. Moreover, the Pechini sol–gel method has been proposed, as a soft chemical method, for the preparation of various nanomaterials.[40,41] This method has

Chemistry Department, Faculty of Science, Benha University, Benha 13518, Egypt. E-mail: m_y_nassar@yahoo.com; m_y_nassar@fsc.bu.edu.eg; Tel: +20 1068727555

several advantages such as its low-cost, low-temperature operation, simplicity, controllable parameters, and homogenous blending at the molecular level.[40,42] However, the Pechini method has not been reported for the synthesis of TiO_2/ZnO nanocomposites so far, to the best of our knowledge. It is noteworthy that the Pechini sol–gel method is a two-step process.[42] The first step is complexation of the metal cations using an organic chelating agent such as citric acid (CA) or ethylenediaminetetraacetic acid (EDTA). The second step is esterification of the produced metal complex using a polyhydroxyl alcohol such as ethylene glycol (EG) forming a polymeric and crosslinked resin. By this way, we can get a homogenous mixture of the used metal cations and less probable segregation of the cations during the ignition process of the polymeric resin which may occur at *ca.* 300 °C. Additionally, it was reported recently that ZnO/Zn_2TiO_4/thin carbon layer composites was an efficient photocatalyst under solar light.[43] Hence, this discussion stimulated us to fabricate TiO_2/Zn_2TiO_4/ZnO/C nanocomposite at a relatively low temperature *via* a Pechini method as a new route for this nanomaterial which was suitable for photocatalytic applications.

In the present study, we have developed a new strategy to synthesize TiO_2/Zn_2TiO_4/ZnO/C nanocomposite as an efficient photocatalyst *via* a facile and low-cost Pechini sol–gel method. Therefore, TiO_2/Zn_2TiO_4/ZnO/activated carbon nanocomposite was prepared using $TiCl_4$, $ZnNO_3$, citric acid (CA), and ethylene glycol (EG). The influence of Ti : Zn molar ratios on the products and the photocatalytic efficiency of the photocatalysts for the degradation of Orange G (OG) dye have been investigated under sunlight and UV irradiation, separately.

2. Experimental

2.1. Materials and reagents

All materials and reagents were of analytical grade and used as received without further purification. Titanium tetrachloride 98% ($TiCl_4$), zinc nitrate ($Zn(NO_3)_2 \cdot 6H_2O$), TiO_2 nanopowder (Degussa (P25)), and Orange G dye (OG; $C_{18}H_{10}N_2O_7Na_2$) were purchased from Sigma-Aldrich Chemical Co. Ammonium hydroxide solution (33%), citric acid (CA, $C_6H_8O_7$), ethylene glycol (EG, $C_2H_6O_2$), hydrogen peroxide 30% (H_2O_2), nitric acid 69% (HNO_3), and hydrochloric acid 37% (HCl) were supplied by El Nasr Pharmaceutical Chemicals Company (Adwic) Company, Cairo, Egypt.

2.2. Preparation of TiO_2/ZnO nanocomposites

An aqueous solution of $TiCl_4$ (2.2 M) in 4 M cold hydrochloric acid solution was prepared, and we used the prepared titanium tetrachloride solution in the subsequent experiments. In a typical procedure: ammonium hydroxide aqueous solution was added drop wise to a stirring $TiCl_4$ solution (10 mL, 0.022 mol, 1 eq.) until pH reached 9 which resulted in white precipitate of $TiO(OH)_2$. The produced $TiO(OH)_2$ precipitate was *in situ* converted into $TiO(NO_3)_2$ solution by addition of a calculated amount of nitric acid; then, few drops of hydrogen peroxide were added to the stirring reaction blend to facilitate the solubility producing a red-orange homogenous solution. 20 mL of an aqueous solution of zinc nitrate (6.545 g, 0.022 mol, 1 eq.) was then added to the stirring red-orange solution so that the Ti : Zn molar ratio was 1 : 1. The solution was then heated up at *ca.* 60 °C. To this hot and stirring solution, 50 mL of citric acid aqueous solution (12.68 g, 0.066 mol, 3 eq.) was added. Afterward, ethylene glycol (8.195 g, 0.132 mol, 6 eq.) was added. After complete dissolution, the temperature was then raised to 120 °C. The molar ratio of total metal cations, M (M = Ti + Zn), citric acid (CA), and ethylene glycol (EG) was 1 : 3 : 6, respectively. The reaction mixture was continued to stir and heat at 120 °C until it turned into viscous polymeric gel. The gel was then burned at 300 °C for 10 min giving brownish-black porous foam. The porous residue was grounded into powder then calcined at 550 °C for 30 min to get rid of the carbonaceous materials producing off-white nanocomposite product. The product was referred to as TZ11. Similar experiments were repeated with constant M : CA : EG molar ratios (*i.e.* 1 : 3 : 6) and varying Ti : Zn molar ratios: 1 : 0, 9 : 1, 7 : 3, 3 : 7, 1 : 9, and 0 : 1. The products were then denoted as T, TZ91, TZ73, TZ37, TZ19, and Z, respectively.

2.3. Characterization

The phase compositions of the products were investigated by powder X-ray diffraction (XRD) measurement on an X-ray diffractometer; Bruker, model D8 Advance, with Cu-Kα radiation; λ = 1.54178 Å. Morphologies of the products were examined by a field-emission scanning electron microscope (FE-SEM; JEOL JSM-6390) and a high-resolution transmission electron microscope (HR-TEM; JEM-2100) operated at an accelerating voltage of 200 kV. The thermal stability of the samples was studied under N_2 atmosphere employing a thermal analyzer equipment (Shimadzu; model TA-60WS), and the heating rate of this analysis was 10 °C min^{-1}. The chemical composition of the products was also investigated using Fourier transform infrared spectra gathered in 4000–200 cm^{-1} range on an FT-IR spectrometer (FT-IR; Thermo Scientific, model Nicolet iS10). The UV-Vis diffuse reflectance spectra of as-prepared samples were performed in the range of 200–800 nm (using barium sulfate as a reference) using UV-visible spectrophotometer (Jasco, model v670) connected to an integral sphere (Jasco, model ISN-723). The UV-Vis spectra of the adsorption and photocatalytic studies of the textile dye under study were performed on a Jasco UV-visible spectrophotometer (UV-Vis; Jasco, model v670).

2.4. Photocatalytic studies

The photocatalytic activity study of the as-prepared products was performed by degradation of Orange G (OG) dye. The photocatalytic degradation was carried out under sunlight illumination by placing the beaker containing the dye solution in a sunny place or under UV irradiation using UV lamps (Philips at 365 nm 4 × 20 watt). The photocatalytic experiments were carried out at room temperature as follows: 50 mg of the as-prepared catalyst was dispersed in 50 mL of Orange G dye solution (20 mg L^{-1}) and allowed to magnetically stir for 1 h in dark to reach an adsorption–desorption equilibrium. Afterward,

the suspension was continued to stir and undergone UV or sunlight irradiation for a specific period. At pre-defined intervals, aliquots were withdrawn and centrifuged to remove the catalyst. The remaining concentration of the dye was determined employing a Jasco UV-visible spectrophotometer (UV-Vis; Jasco, model v670). The kinetics of the photocatalytic degradation processes of the dye was discussed as well. The degradation efficiency (DE) was estimated using the following relationship:

$$\mathrm{DE} = \frac{C_0 - C_t}{C_0} \times 100\% \quad (1)$$

where, C_0 and C_t are the initial concentration of the dye at zero time (*i.e.* before illumination) and the remaining concentration of the dye after illumination for time t, respectively.

3. Results and discussion

3.1. Synthesis and characterization of the as-prepared photocatalysts

3.1.1. XRD investigation. The crystal structures of the generated TiO_2, ZnO, and TiO_2/ZnO nano-composite products – from simple and inexpensive precursors *via* a facile Pechini sol–gel route – calcined at 550 °C were investigated using the XRD patterns. The XRD results are presented in Fig. 1(a–g). Fig. 1(a) exhibited the XRD pattern of pure tetragonal anatase TiO_2 product, T, (JCPDS file no. 01-071-1168) indicating the high efficiency of the exploited Pechini sol–gel method in producing pure anatase TiO_2 nanoparticles.[44] No peaks from other crystalline impurities have been detected. The results also revealed that the used Pechini route produced pure ZnO nanoparticles because the diffraction peaks of the generated sample, Z, (Fig. 1(g)) could be indexed well to a pure hexagonal crystalline phase of ZnO (JCPDS file no. 01-071-1168).[45] No reflection patterns from other crystalline impurities have been observed. On the other hand, using various Ti : Zn molar ratios during the preparation method, as shown in Fig. 1(b–f), generated various TiO_2/ZnO_2 nano-composites: TZ91, TZ73, TZ11, TZ37, and TZ19. The XRD patterns of the products: TZ73, TZ11, and TZ37, showed the existence of diffraction peaks corresponding to the formation of both tetragonal anatase TiO_2 (JCPDS file no. 01-071-1168) and hexagonal crystalline phase of ZnO (JCPDS file no. 01-071-1168) as a mixture. However, TZ91 and TZ19 samples did not exhibit the diffraction peaks of both TiO_2 and ZnO phases as a mixture but the samples showed the XRD patterns of TiO_2 and ZnO phases, respectively. This can be attributed to that all the ZnO is incorporated in the TiO_2 lattice in the TZ91 sample and *vice versa* for the TZ19 sample resulting in that ZnO peaks cannot be detected in TZ91 and TiO_2 peaks have not been observed in TZ19. This could also be deduced from the broadness of the diffraction peaks of both samples. Moreover, this was also supported by the FT-IR spectroscopy, as will be shortly explained. This behavior is consistent with the findings of Janitabar-Darzi.[46] Interestingly, 7 : 3 and 1 : 1 Ti : Zn molar ratios produced a mixture of TiO_2 and ZnO phases in addition to the appearance of some new reflection peaks attributing to Zn_2TiO_4 phase as shown in Fig. 1(c and d). The new diffraction peaks could be indexed well to a cubic phase of Zn_2TiO_4 (JCPDS file no. 01-077-0014).[47]

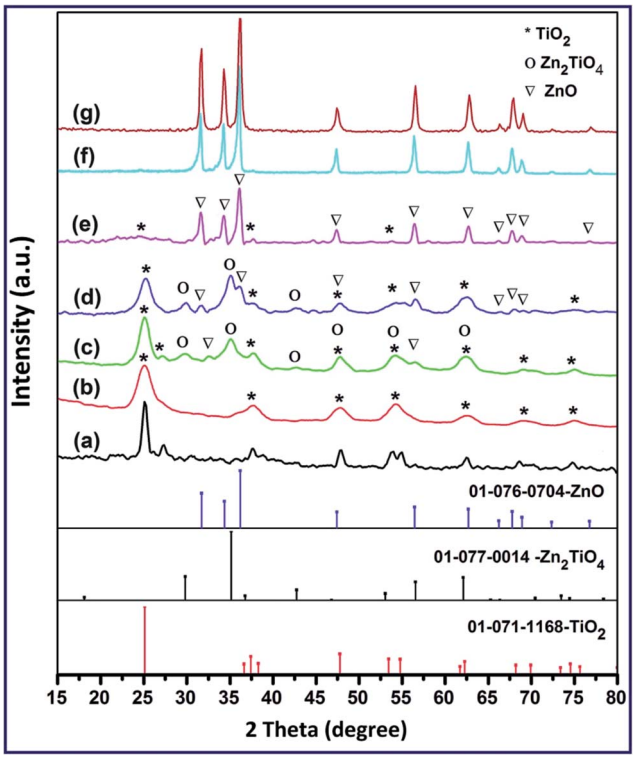

Fig. 1 X-ray diffraction patterns of T (a), TZ91 (b), TZ73 (c), TZ11 (d), TZ37 (e), TZ19 (f) and Z (g) products calcined at 550 °C.

The existence of the new phase (Zn_2TiO_4) may result from the reaction of some of TiO_2 and ZnO phases in the flame of the combustion process, which has a relatively high temperature, at the used molar ratios producing a single solid phase solution of Zn_2TiO_4. This result is in agreement with the results reported by Janitabar-Darzi.[46] Moreover, based on the intensity of the diffraction peaks, the percentages of TiO_2, ZnO, and Zn_2TiO_4 phases were approximately found to be 55.8, 12.2 and 32.0%, respectively, for the TZ73 sample and 38.5, 18.5 and 43.0%, respectively, for the TZ11 sample. Additionally, the average crystallite sizes of the products calcined at 550 °C were estimated using the Debye–Scherrer equation (eqn (2)).[48]

$$D = 0.9\lambda/\beta \cos \theta_B \quad (2)$$

where, θ_B, β, and λ are, the Bragg diffraction angle, diffraction peak full width at half maximum (FWHM), and wavelength of the X-ray radiation (nm), respectively. The average crystallite size of the T, TZ91, TZ73, TZ11, TZ37, TZ19 and Z products was estimated to be 20, 38, 29, 30, 49, 66, and 70 nm, respectively.

3.1.2. FT-IR investigation. Chemical compositions of the as-synthesized products calcined at 550 °C were investigated using the FT-IR spectroscopy and the FT-IR spectra are depicted in Fig. 2. Fig. 2(a) evinced four vibrational absorptions at 347, 462, 503, and 750 cm^{-1} characteristic to Ti–O bond of the TiO_2 product.[49,50] Fig. 2(g) showed two characteristic IR bands for ZnO at 436 and 500 cm^{-1}. These results are in good agreement with the reported data.[9,49–51] Moreover, Fig. 2(b–f) revealed the

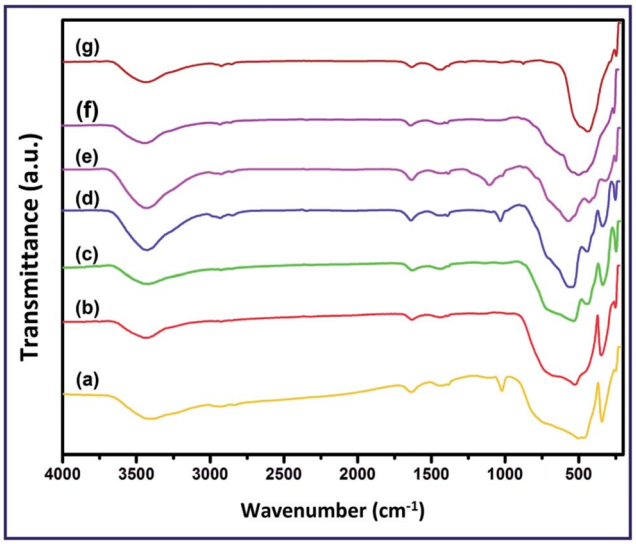

Fig. 2 FT-IR spectra of T (a), TZ91 (b), TZ73 (c), TZ11 (d), TZ37 (e), TZ19 (f) and Z (g) products calcined at 550 °C.

characteristic vibrations at *ca.* 338, 427, 490, 555, and 723 cm^{-1} attributing to Zn–O and Ti–O of TiO_2/ZnO composites which are consistent with the reported results.[50,51] In addition to, Fig. 2(c and d) showed medium vibrational bands at about 334, 441, and 541 cm^{-1} along with the previously mentioned bands for TiO_2/ZnO composites corresponding to the formation of Zn_2TiO_4 phase. These data are consistent with the published data.[50,52–54] However, the FT-IR spectra of the as-prepared products, except TZ91 and TZ73, evinced weak bands at *ca.* 1025 and 1429 cm^{-1} owing to the presence of small amount of the organic residue in the prepared products.[54–56] Moreover, Fig. 2 exhibited vibrational bands at *ca.* 1635 and 3415 cm^{-1} corresponding to bending and stretching frequencies, respectively, of the OH– groups of the adsorbed water molecules.[18,57,58] Eventually, the FT-IR results are summarized in Table 1.

3.1.3. Thermal investigation. Thermal analyses (TG/DTG/DSC) of the combustion products (T, TZ73, and Z), before calcination, have been investigated and depicted in Fig. 3(a–c). The three combustion products were taken as representative examples. The TG curves, Fig. 3(ai–ci), of the combustion products; T and TZ73, exhibited weight losses of 4 and 2%, respectively, in the temperature range of *ca.* 50–200 °C attributing to the removal of the physically adsorbed water molecules. Besides, the TG curves, Fig. 3(ai–ci), revealed sharp weight losses of 58, 49, and 31% in the temperature range of *ca.* 250–500 °C, for the aforementioned products, respectively, corresponding to decomposition of the remaining organic residue after the combustion process.

The TG analysis was supported by DTG (Fig. 3(aii–cii)) and DSC (Fig. 3(aiii–ciii)) analyses since both analyses showed two peaks for T and TZ73 products and only one exothermic peak for Z product. The first one was very broad and weak due to the elimination of the adsorbed water molecules and this step was endothermic according to the DSC curves (Fig. 3(aiii–ciii)). The second peak for all samples in both analyses was sharp and exothermic peak based on the DSC curves (Fig. 3(aiii–ciii)), and this peak appeared at *ca.* 467, 461 and 437 °C, respectively, for the previously mentioned combustion products. It is noteworthy that, according to thermal analysis results, it can be deduced that the calcination temperature of 550 °C will be enough to produce pure ZnO, TiO_2, Zn_2TiO_4, and ZnO/TiO_2 products.

3.1.4. Morphology investigation. Morphology of the combustion products: T, TZ73, and Z, calcined at 550 °C has been investigated utilizing a field-emission scanning electron microscope (FE-SEM) as presented in Fig. 4(a–c), respectively. The low magnification FE-SEM images (Fig. 4(ai–ci)) of the products exhibited that the products: T, TZ73, and Z, are composed of irregular shape flakes with an approximate size of 2.5, 5, and 2.5 μm, respectively. Moreover, high magnification FE-SEM images (Fig. 4(aii–cii)) reveal the porosity feature of the all synthesized products. Besides, the irregular shape flakes of the all prepared samples are composed of agglomerations of spherical and irregular shape nanoparticles. However, TZ73 sample contains some black spots which may be attributing to the presence of some carbon residue along with the ZnO/Zn_2TiO_4/TiO_2 composite particles. Fig. 5(a–c) exhibits the EDX spectra of the as-prepared products (T, TZ73, and Z) calcined at 550 °C and the spectra confirm the purity of the prepared oxides. The EDX spectrum of T product (Fig. 5(a)) revealed Ti and O elements proving the existence of TiO_2 particles. Besides, the spectrum of Z product (Fig. 5(c)) showed Zn and O elements supporting the formation of ZnO particles. And the EDX spectrum (Fig. 5(b)) of TZ73 product exhibited Ti, Zn, O, and C elements confirming the formation of TiO_2/ZnO and Zn_2TiO_4 particles and the presence of small quantity of carbon residue.

Consequently, combined with the XRD and FT-IR results, it was confirmed that TiO_2, ZnO, and TiO_2/Zn_2TiO_4/ZnO/activated carbon nano-composite products have been successfully

Table 1 IR vibrational frequencies of the as-prepared products

Product	Label	ν_{Ti-O}, cm^{-1}	ν_{Zn-O}, cm^{-1}	ν_{TiOZn}, cm^{-1}	ν_{C-O}, cm^{-1}	ν_{CH_2}, cm^{-1}	ν_{OH}, cm^{-1}	δ_{OH}, cm^{-1}
TiO_2	T	347, 462, 503, 750	—	—	1025	1429	3415	1635
$9TiO_2$: 1ZnO	TZ91	338, 723, 555	427, 490	—	—	1429	3415	1635
$7TiO_2$: 3ZnO	TZ73	338, 723, 555	427, 490	334, 441, 541	—	1429	3415	1635
$1TiO_2$: 1ZnO	TZ11	338, 723, 555	427, 490	334, 441, 541	1025	1429	3415	1635
$3TiO_2$: 7ZnO	TZ37	338, 723, 555	427, 490	—	1070	1429	3415	1635
$1TiO_2$: 9ZnO	TZ19	338, 723, 555	427, 490	—	1025	1429	3415	1635
ZnO	Z	—	436, 500	—	1025	1429	3415	1635

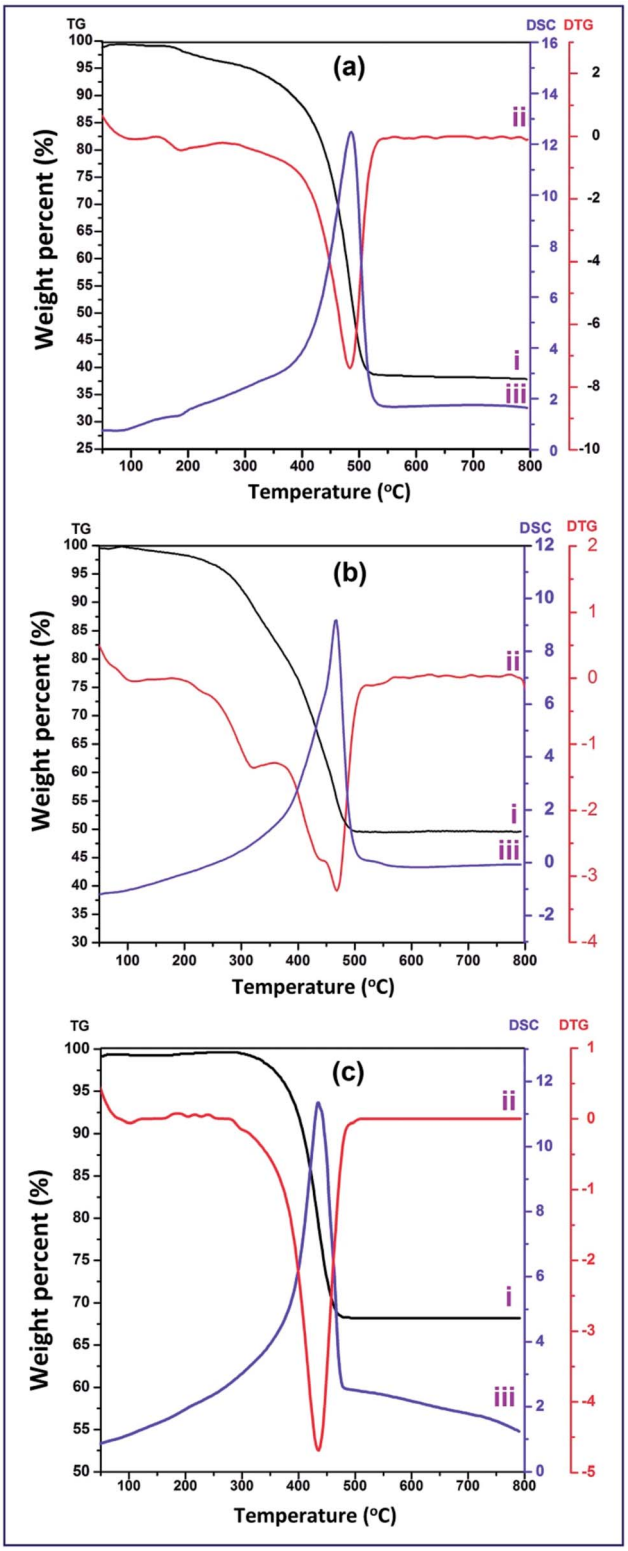

Fig. 3 Thermal analyses (TGA, DSC and DTG curves) of T (a), TZ73 (b), and Z (c) samples.

synthesized. Moreover, microstructures of the combustion products: T, TZ73, and Z, were examined employing a transmission electron microscope (TEM), Fig. 6(a–c). The TEM images of the samples exhibited that the three samples have similar morphologies since they all are composed of spherical, square-like, and irregular particles. Besides, the TEM images of the as-prepared samples showed the porous nature of the products. However, the obtained average particle sizes were 21, 31, and 74 nm for T, TZ73, and Z products, respectively, which are in good agreement with the XRD results.

3.2. Investigation of the photocatalytic activity of the as-prepared catalysts

The photocatalytic properties of the as-synthesized products: T, TZ91, TZ73, TZ11, TZ37, TZ19 and Z, have been investigated by examining the degradation of the OG dye under sunlight and UV irradiation, separately. The results are displayed in Fig. 7(a and b), respectively. The results revealed that OG degradation under sunlight illumination in the absence of photocatalyst was very slow. However, in the presence of the photocatalyst, the dye degraded significantly in a short time. It is clear that the photocatalytic degradation of the OG dye over TZ73 nanocomposite is higher than those over the other prepared nanocatalysts (Ti, TZ91, TZ11, TZ37, TZ19, and Z), under sunlight illumination. Moreover, degradation of the OG dye over TZ73 nanocomposite under sunlight irradiation is also higher than that over the commercially available TiO_2 (P25). Interestingly, degradation of the OG dye reached *ca.* 100% after 50 min irradiation time over TZ73 nanocomposite. On the other hand, carrying out similar experiments under UV irradiation exhibited that OG degraded slowly until it reached about 40% after 180 min. However, the degradation of OG dye was enhanced significantly in the presence of photocatalysts, under UV illumination. The results revealed that degradation of the OG dye was also higher in the presence of TZ73 nanocomposite and it reached *ca.* 100% in 120 min in comparison to the other prepared photocatalysts (P25, Ti, TZ91, TZ11, TZ37, TZ19, and Z), under UV irradiation. The UV-Vis spectra of the degraded dye under investigation (not shown here) exhibited that absorbance of the absorption peak decreased with increasing the time of irradiation without any change in the peak position. Besides, the spectra of the degraded dye did not show new peaks during the photocatalytic degradation. Consequently, it could be concluded that decomposition mechanism of the OG dye degradation proceeded through an aromatic ring opening mechanism and not through the formation of different stable intermediates.[59,60]

Additionally, the photocatalytic degradation of OG dye over the as-prepared photocatalysts was quantitatively investigated using the pseudo-first-order kinetic model, and the observed first-order rate constant (k_{obs}) was determined. The values of the calculated k_{obs} constants are presented in Fig. 8(a and b), for the sunlight and UV irradiation, respectively. The kinetic data revealed that the degradation rate constants over P25, Ti, TZ91, TZ73, TZ11, TZ37, TZ19, and Z products under sunlight irradiation were 3.855×10^{-3}, 36.29×10^{-3}, 47.93×10^{-3}, 113.48×10^{-3}, 54.56×10^{-3}, 21.37×10^{-3}, 13.95×10^{-3}, and 2.300×10^{-3} min^{-1}, respectively. Hence, the activity of TZ73 nanocomposite (*i.e.* $TiO_2/Zn_2TiO_2/ZnO$/activated carbon) is about 29.4, 3.13, 2.37, 2.07, 5.31, 8.13, and 49.3-folds higher than those of P25, Ti, TZ91, TZ11, TZ37, TZ19, and Z products,

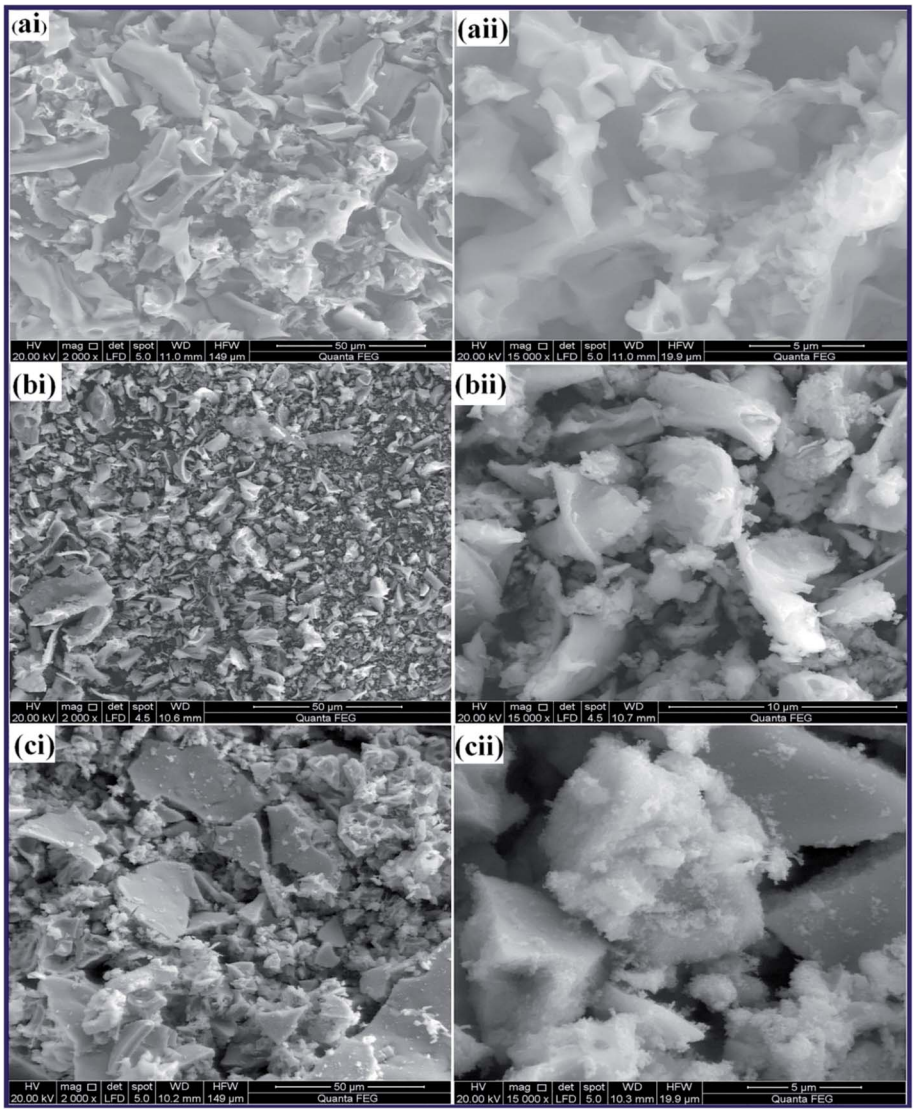

Fig. 4 FE-SEM images of T (a), TZ73 (b), and Z (c) products calcined at 550 °C.

respectively. This means that presence of TiO_2 and ZnO in contact at a molar ratio of 7 : 3 and coexistence of $ZnTiO_4$ and activated carbon as well resulted in a photocatalyst with the highest activity. Similar results were obtained for investigation of the as-prepared products under UV illumination. The kinetic results exhibited that the degradation rate constants over P25, Ti, TZ91, TZ73, TZ11, TZ37, TZ19, and Z products under UV irradiation were 4.990×10^{-3}, 13.18×10^{-3}, 13.04×10^{-3}, 29.46×10^{-3}, 25.02×10^{-3}, 18.34×10^{-3}, 13.88×10^{-3}, and 12.61×10^{-3} min^{-1}, respectively. Consequently, the activity of TZ73 nanocomposite is *ca.* 5.90, 2.24, 2.26, 1.18, 1.61, 2.12, and 2.34-folds higher than those of P25, Ti, TZ91, TZ11, TZ37, TZ19, and Z samples. Therefore the TZ73 sample was the photocatalyst that has the highest catalytic activity. However, according to the obtained results, the activity of the as-prepared photocatalyst under sunlight illumination was 3.85-fold higher than its activity under UV illumination. We obtained similar results for the photocatalytic degradation of Reactive Red 195 dye over magnesium aluminate photocatalyst where the activity of the photocatalyst was higher under sunlight illumination compared to its activity under UV illumination.[17]

Moreover, the high photocatalytic activity of the composite TZ73 may be due to the generation of more electron–hole pairs in this composite and the ability of this composite to efficiently suppress the recombination of electron–hole pairs because of the coexistence of TiO_2, ZnO, Zn_2TiO_4, and carbon phases together resulting in high separation efficiency of charge carriers. To illustrate the efficiency of separation of charge carriers for TiO_2/ZnO/Zn_2TiO_4/carbon nanocomposite, the conduction (CB) and valence (VB) band positions for TiO_2, ZnO, and Zn_2TiO_4 were calculated employing eqn (3) and (4),[61–63] and the results are presented in Fig. 9(a)

$$E_{CB} = XE^{e} - 0.5E_{g} \quad (3)$$

$$E_{VB} = E_{C} + E_{g} \quad (4)$$

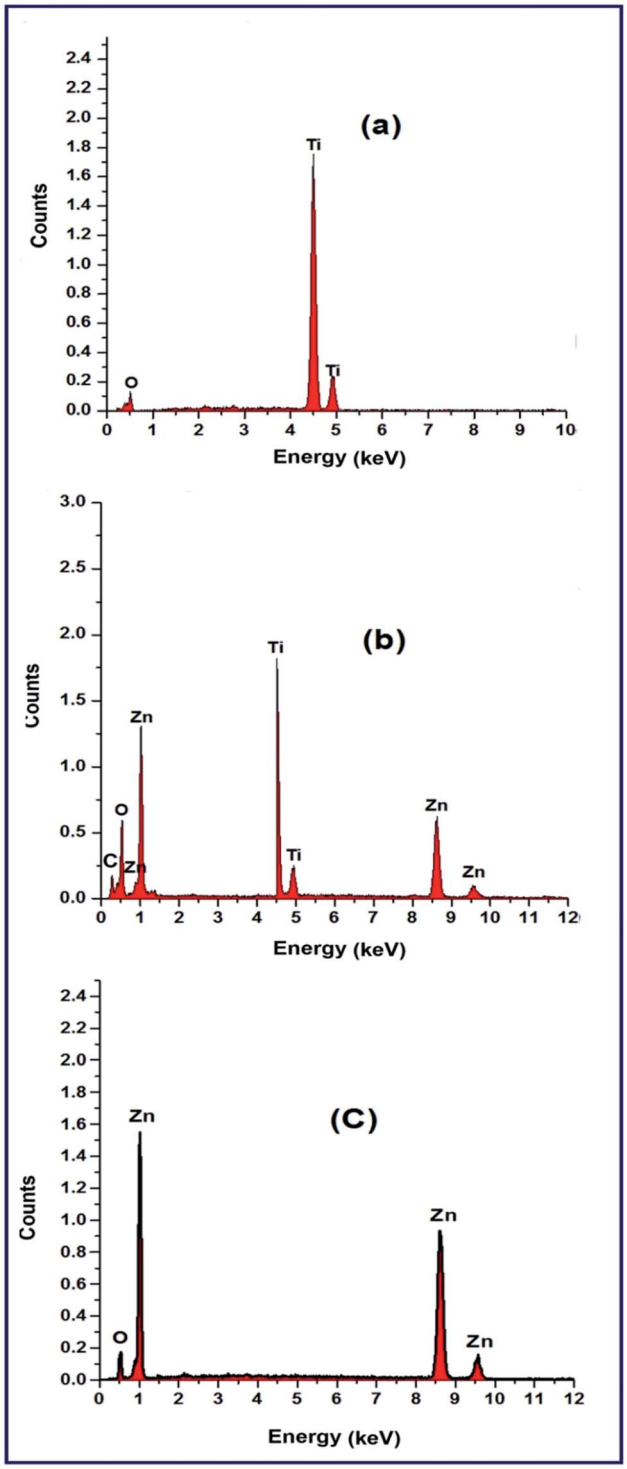

Fig. 5 EDX spectra of T (a), TZ73 (b), and Z (c) products calcined at 550 °C.

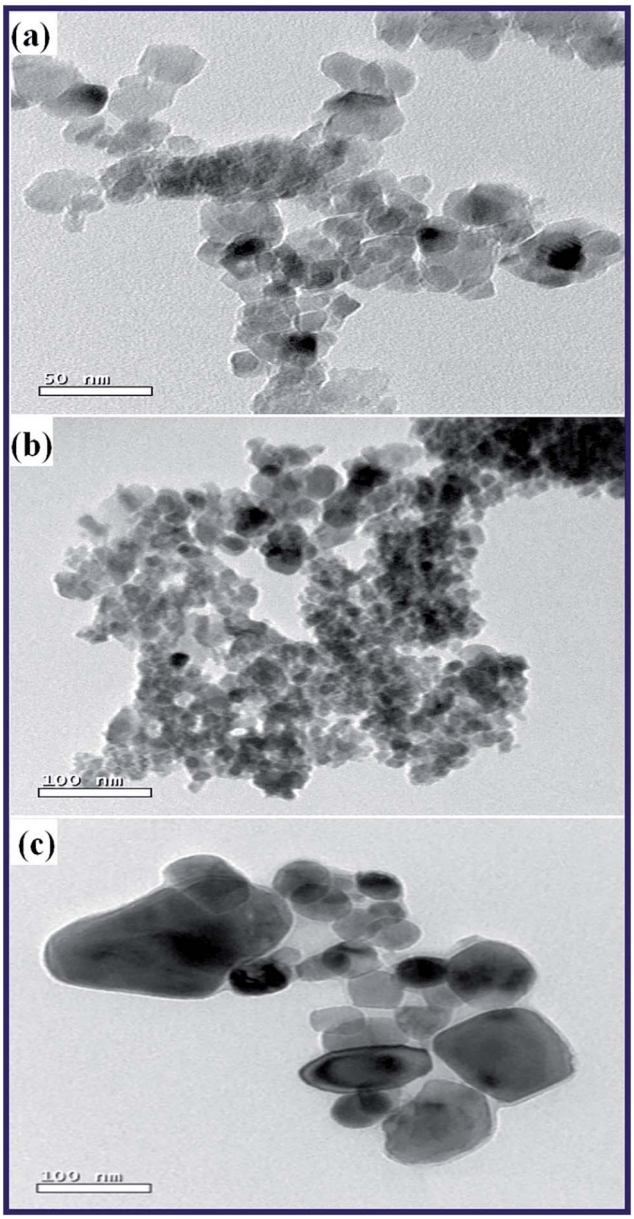

Fig. 6 TEM images of T (a), TZ73 (b), and Z (c) products calcined at 550 °C.

where X is the absolute electronegativity, E^e is the energy of free electrons on the hydrogen scale (4.5 eV), and E_g is the band gap energy of the semiconductor. The reported E_g and our calculated values based on the UV-Vis diffuse reflectance spectra (not shown here) for TiO_2 and ZnO were found to be *ca.* 3.2 eV, and the reported value for Zn_2TiO_4 was found to be 4.01 eV.[51,64] The estimated VB and CB energies for TiO_2, ZnO, and Zn_2TiO_4 were found to be (2.86 and −0.34 eV), (2.91 and −0.29 eV), and (3.305 and −0.705 eV), respectively. Moreover, the estimated energy positions of VB and CB for carbon thin layer were reported by Lim *et al.*[43] According to the estimated values of VB and CB (Fig. 9(a)) for phases forming the nanocomposite TZ73, under irradiation, the electrons absorb light and transfer through excitation from VBs of carbon thin layer, TiO_2, ZnO, and Zn_2TiO_4 to their corresponding CBs. Additionally, energies of CBs carbon thin layer and Zn_2TiO_4 are more negative than those for the other composite components; TiO_2 and ZnO. Consequently, the photogenerated electrons on the CB of carbon thin layer flow to CB of Zn_2TiO_4, and the photogenerated electrons on the CB of Zn_2TiO_4 will also flow to CB of ZnO then to CB of

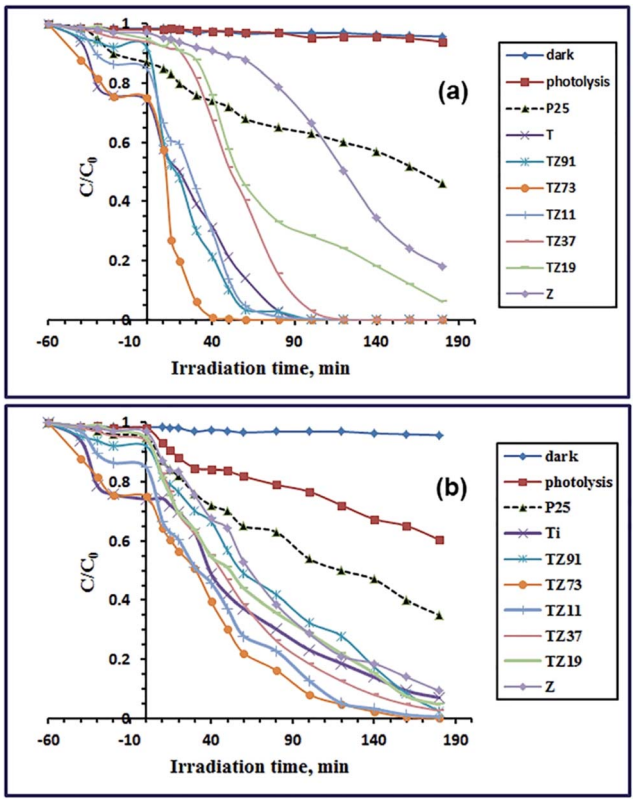

Fig. 7 Photocatalytic degradation of OG dye solution over P25, Ti, TZ91, TZ73, TZ11, TZ37, TZ19, and Z products under sunlight (a) and UV (b) irradiation.

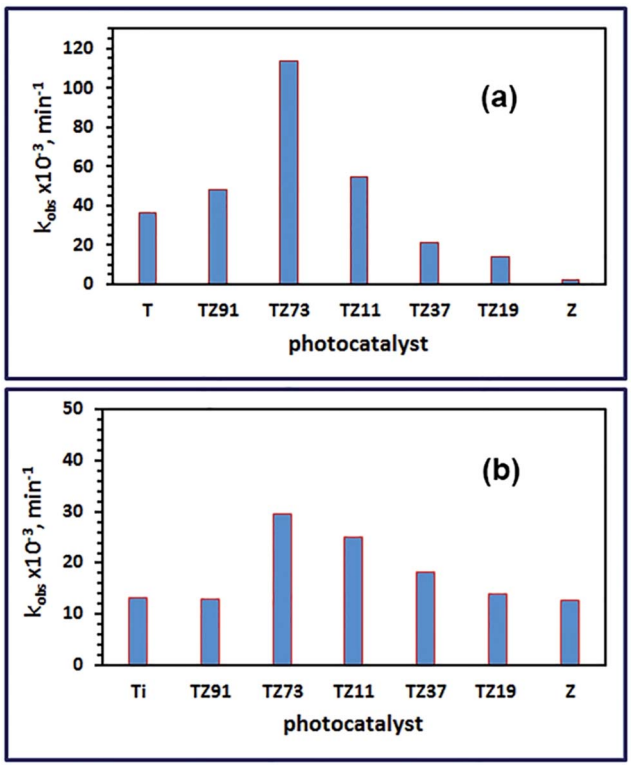

Fig. 8 The degradation rate constants of OG dye over P25, Ti, TZ91, TZ73, TZ11, TZ37, TZ19, and Z products under sunlight (a) and UV (b) irradiation.

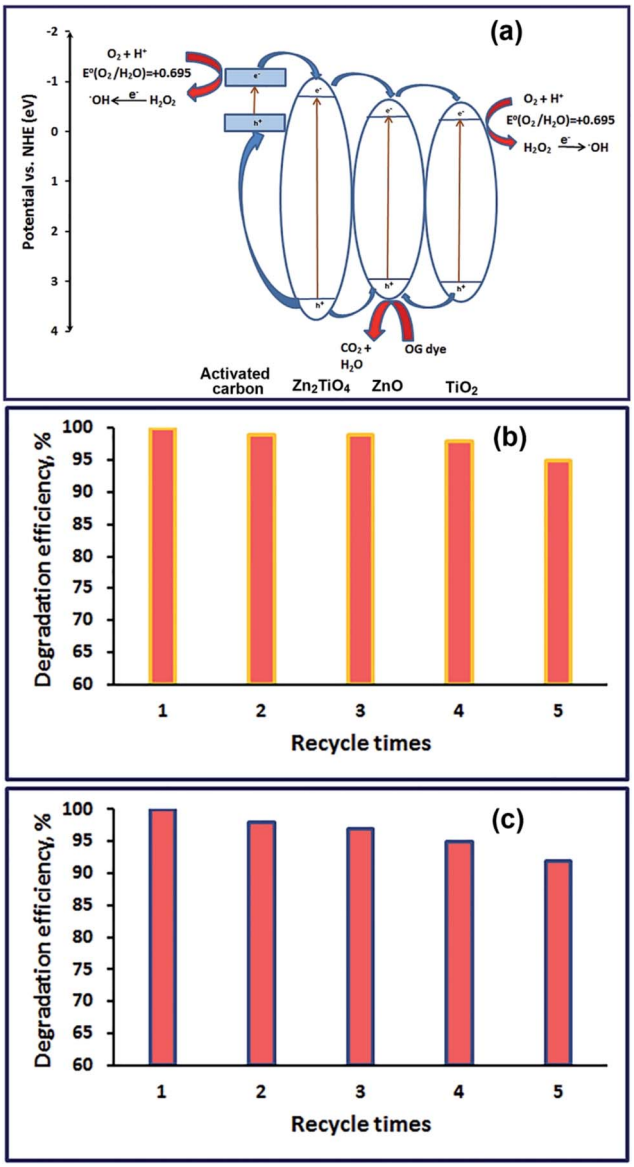

Fig. 9 The proposed degradation mechanism of OG dye over TZ73 nanocomposite (a), reusability of the TZ73 nanocomposite for five successive times under sunlight (b) and UV (c) irradiation.

TiO_2. Moreover, the photogenerated holes flow from VB of TiO_2 to that of ZnO and from VB of Zn_2TiO_4 to those of ZnO and carbon thin layer. Hence, electrons are gathered on the CB of TiO_2 and holes on VBs of ZnO and carbon thin layer, resulting in efficient charge separations. Moreover, the CBs potential of carbon thin layer and Zn_2TiO_4 are more negative than that of $O_2/{}^{\bullet}O_2^-$ (−0.33 eV); consequently, O_2 molecules will probably be converted into superoxide radical (${}^{\bullet}O_2^-$) over the activated carbon residue, consistent with the reported results,[65] and over Zn_2TiO_4. However, similar reduction reactions did not occur on the CB of ZnO and TiO_2 phases. Moreover, the potential of O_2/H_2O_2 reaction is more positive than those of CB energies of activated carbon residue, Zn_2TiO_4, TiO_2, and ZnO. Hence, the adsorbed molecular oxygen can react with the photogenerated electrons on their CBs producing H_2O_2 which in turn can be

decomposed by reacting with the photogenerated electrons generating $^{\bullet}OH$ radicals. On the other hand, oxidation of H_2O ($E^0(H_2O/^{\bullet}OH) = +2.72$ eV) and –OH ($E^0(OH/^{\bullet}OH) = +2.38$ eV) to $^{\bullet}OH$ radicals does not occur on the components of the nanocomposite (TZ73) owing to their VBs values. Therefore, the adsorbed dye molecules will react with the photogenerated holes resulting in dye degradation into small molecules, *e.g.*, H_2O and CO_2.[66] It is noteworthy that similar behavior for photocatalytic degradation of some organic dyes over ZnO/Zn_2TiO_4 under solar light irradiation has been reported recently.[43]

The efficiency of the as-synthesized TZ73 nanocomposite was examined by studying its reusability for OG dye degradation. Therefore, successive photocatalytic degradation reactions over TZ73 nanocomposite was achieved under sunlight and UV illumination, and the results were presented in Fig. 9(b and c), respectively. The results reveal that the photocatalytic activity of the photocatalyst remains almost constant even after four cycles, indicating the stability of the photocatalyst in the degradation reactions under sunlight and UV irradiation.

4. Conclusions

In conclusion, a novel quaternary $TiO_2/Zn_2TiO_2/ZnO/C$ nanocomposite was successfully prepared *via* a facile Pechini sol–gel method. The crystallite sizes and composition phases of the products have been tuned by using various the Ti^{4+} : Zn^{2+} molar ratios during the preparation process. The as-prepared products: TiO_2, ZnO, TiO_2/ZnO, and $TiO_2/Zn_2TiO_2/ZnO$/activated carbon, exhibited good photocatalytic activity for the removal of Orange G dye under sunlight and under UV irradiation. However, the as-prepared $TiO_2/Zn_2TiO_2/ZnO$/activated carbon photocatalyst showed the highest efficiency for the removal of OG dye. The dye removal percentage through the photocatalytic degradation over $TiO_2/Zn_2TiO_2/ZnO/C$ photocatalyst reached *ca.* 100% in 50 and 120 min, under sunlight and UV illumination, respectively. Moreover, the results indicated the stability and reusability of the as-prepared nanocomposite and its applicability for the removal of OG textile dye removal from aqueous solutions. However, based on the promising findings presented in this paper, work on the remaining issues is continuing, and it will be reported in a future paper.

Acknowledgements

The first author thanks Benha University – Egypt, for financial support of the current research.

References

1 W. Wang, T. Jiao, Q. Zhang, X. Luo, J. Hu, Y. Chen, Q. Peng, X. Yan and B. Li, Hydrothermal synthesis of hierarchical core–shell manganese oxide nanocomposites as efficient dye adsorbents for wastewater treatment, *RSC Adv.*, 2015, **5**, 56279–56285.
2 T. A. Khan, S. Dahiya and I. Ali, Use of kaolinite as adsorbent: Equilibrium, dynamics and thermodynamic studies on the adsorption of rhodamine B from aqueous solution, *Appl. Clay Sci.*, 2012, **69**, 58–66.
3 M. Y. Nassar, A. S. Amin, I. S. Ahmed and S. Abdallah, Sphere-like Mn_2O_3 nanoparticles: Facile hydrothermal synthesis and adsorption properties, *J. Taiwan Inst. Chem. Eng.*, 2016, **64**, 79–88.
4 M. Y. Nassar, I. S. Ahmed, T. Y. Mohamed and M. Khatab, A controlled, template-free, and hydrothermal synthesis route to sphere-like [small alpha]-Fe_2O_3 nanostructures for textile dye removal, *RSC Adv.*, 2016, **6**, 20001–20013.
5 N. F. Cardoso, R. B. Pinto, E. C. Lima, T. Calvete, C. V. Amavisca, B. Royer, M. L. Cunha, T. H. M. Fernandes and I. S. Pinto, Removal of remazol black B textile dye from aqueous solution by adsorption, *Desalination*, 2011, **269**, 92–103.
6 M. Y. Nassar, E. I. Ali and E. S. Zakaria, Tunable autocombustion preparation of TiO_2 nanostructures as efficient adsorbents for the removal of an anionic textile dye, *RSC Adv.*, 2017, **7**, 8034–8050.
7 H. Guo, T. Jiao, Q. Zhang, W. Guo, Q. Peng and X. Yan, Preparation of Graphene Oxide-Based Hydrogels as Efficient Dye Adsorbents for Wastewater Treatment, *Nanoscale Res. Lett.*, 2015, **10**, 1–10.
8 T. Jiao, Y. Liu, Y. Wu, Q. Zhang, X. Yan, F. Gao, A. J. P. Bauer, J. Liu, T. Zeng and B. Li, Facile and Scalable Preparation of Graphene Oxide-Based Magnetic Hybrids for Fast and Highly Efficient Removal of Organic Dyes, *Sci. Rep.*, 2015, **5**, 12451.
9 M. Y. Nassar, M. M. Moustafa and M. M. Taha, Hydrothermal tuning of the morphology and particle size of hydrozincite nanoparticles using different counterions to produce nanosized ZnO as an efficient adsorbent for textile dye removal, *RSC Adv.*, 2016, **6**, 42180–42195.
10 J. Huang, Y. Cao, Z. Liu, Z. Deng and W. Wang, Application of titanate nanoflowers for dye removal: A comparative study with titanate nanotubes and nanowires, *Chem. Eng. J.*, 2012, **191**, 38–44.
11 M. Y. Nassar and I. S. Ahmed, Template-free hydrothermal derived cobalt oxide nanopowders: Synthesis, characterization, and removal of organic dyes, *Mater. Res. Bull.*, 2012, **47**, 2638–2645.
12 H. R. Mahmoud, S. M. Ibrahim and S. A. El-Molla, Textile dye removal from aqueous solutions using cheap MgO nanomaterials: Adsorption kinetics, isotherm studies and thermodynamics, *Adv. Powder Technol.*, 2016, **27**, 223–231.
13 R. G. Saratale, G. D. Saratale, J. S. Chang and S. P. Govindwar, Bacterial decolorization and degradation of azo dyes: A review, *J. Taiwan Inst. Chem. Eng.*, 2011, **42**, 138–157.
14 M. Y. Nassar and S. Abdallah, Facile controllable hydrothermal route for porous $CoMn_2O_4$ nanostructure: Synthesis, characterization, and textile dye removal from aqueous media, *RSC Adv.*, 2016, **6**, 84050–84067.
15 M. Y. Nassar and M. Khatab, Cobalt ferrite nanoparticles *via* a template-free hydrothermal route as an efficient nano-adsorbent for potential textile dye removal, *RSC Adv.*, 2016, **6**, 79688–79705.

16 H. M. Aly, M. E. Moustafa, M. Y. Nassar and E. A. Abdelrahman, Synthesis and characterization of novel Cu(II) complexes with 3-substituted-4-amino-5-mercapto-1,2,4-triazole Schiff bases: A new route to CuO nanoparticles, *J. Mol. Struct.*, 2015, **1086**, 223–231.

17 M. Y. Nassar, I. S. Ahmed and I. Samir, A novel synthetic route for magnesium aluminate ($MgAl_2O_4$) nanoparticles using sol–gel auto combustion method and their photocatalytic properties, *Spectrochim. Acta, Part A*, 2014, **131**, 329–334.

18 M. Y. Nassar, T. Y. Mohamed, I. S. Ahmed and I. Samir, MgO nanostructure *via* a sol–gel combustion synthesis method using different fuels: An efficient nano-adsorbent for the removal of some anionic textile dyes, *J. Mol. Liq.*, 2017, **225**, 730–740.

19 M. Y. Nassar, H. M. Aly, M. E. Moustafa and E. A. Abdelrahman, Synthesis, Characterization and Biological Activity of New 3-substitued-4-amino-5-hydrazino-1,2,4-triazole Schiff Bases and their Cu(II) Complexes: A New Approach to CuO Nanoparticles for Photocatalytic Degradation of Methylene Blue Dye, *J. Inorg. Organomet. Polym. Mater.*, 2017, 1–14.

20 M. Y. Nassar, H. M. Aly, E. A. Abdelrahman and M. E. Moustafa, Synthesis, characterization, and biological activity of some novel Schiff bases and their Co(II) and Ni(II) complexes: A new route for Co_3O_4 and NiO nanoparticles for photocatalytic degradation of methylene blue dye, *J. Mol. Struct.*, 2017, **1143**, 462–471.

21 H. Zhu, R. Jiang, Y. Fu, Y. Guan, J. Yao, L. Xiao and G. Zeng, Effective photocatalytic decolorization of methyl orange utilizing TiO_2/ZnO/chitosan nanocomposite films under simulated solar irradiation, *Desalination*, 2012, **286**, 41–48.

22 C. Wang, H. Liu and Y. Qu, Based Photocatalytic Process for Purification of Polluted Water: Bridging Fundamentals to Applications, *J. Nanomater.*, 2013, **2013**, 14.

23 P. Margan and M. Haghighi, Hydrothermal-assisted sol–gel synthesis of Cd-doped TiO_2 nanophotocatalyst for removal of acid orange from wastewater, *J. Sol-Gel Sci. Technol.*, 2016, 1–14.

24 X. Liu and Y. Bi, *In situ* preparation of oxygen-deficient TiO_2 microspheres with modified {001} facets for enhanced photocatalytic activity, *RSC Adv.*, 2017, **7**, 9902–9907.

25 J. Hu, Y. Cao, K. Wang and D. Jia, Green solid-state synthesis and photocatalytic hydrogen production activity of anatase TiO_2 nanoplates with super heat-stability, *RSC Adv.*, 2017, **7**, 11827–11833.

26 S. Singh, V. C. Srivastava, S. L. Lo, T. K. Mandal and G. Naresh, Morphology-controlled green approach for synthesizing the hierarchical self-assembled 3D porous ZnO superstructure with excellent catalytic activity, *Microporous Mesoporous Mater.*, 2017, **239**, 296–309.

27 T. K. Jana, A. Pal and K. Chatterjee, Self assembled flower like CdS–ZnO nanocomposite and its photo catalytic activity, *J. Alloys Compd.*, 2014, **583**, 510–515.

28 E. A. Araujo Junior, F. X. Nobre, G. D. S. Sousa, L. S. Cavalcante, M. Rita de Morais Chaves Santos, F. L. Souza and J. M. Elias de Matos, Synthesis, growth mechanism, optical properties and catalytic activity of ZnO microcrystals obtained *via* hydrothermal processing, *RSC Adv.*, 2017, **7**, 24263–24281.

29 T. A. Thu Do, H. T. Giang, D. Van Huong, P. Q. Ngan, G. H. Thai, D. T. Thu and T. D. Lam, Correlation between photoluminescence spectra with gas sensing and photocatalytic activities in hierarchical ZnO nanostructures, *RSC Adv.*, 2017, **7**, 9826–9832.

30 G. S. Pozan and A. Kambur, Significant enhancement of photocatalytic activity over bifunctional ZnO–TiO_2 catalysts for 4-chlorophenol degradation, *Chemosphere*, 2014, **105**, 152–159.

31 A. Kubacka, M. Ferrer and M. Fernández-García, Kinetics of photocatalytic disinfection in TiO_2-containing polymer thin films: UV and visible light performances, *Appl. Catal., B*, 2012, **121–122**, 230–238.

32 S. Hernández, V. Cauda, D. Hidalgo, V. Farías Rivera, D. Manfredi, A. Chiodoni and F. C. Pirri, Fast and low-cost synthesis of 1D ZnO–TiO_2 core–shell nanoarrays: Characterization and enhanced photo-electrochemical performance for water splitting, *J. Alloys Compd.*, 2014, **615**(suppl. 1), S530–S537.

33 E. Colombo, W. Li, S. K. Bhangu and M. Ashokkumar, Chitosan microspheres as a template for TiO_2 and ZnO microparticles: studies on mechanism, functionalization and applications in photocatalysis and H_2S removal, *RSC Adv.*, 2017, **7**, 19373–19383.

34 M.-H. Liao, C.-H. Hsu and D.-H. Chen, Preparation and properties of amorphous titania-coated zinc oxide nanoparticles, *J. Solid State Chem.*, 2006, **179**, 2020–2026.

35 M. I. Khan, K. A. Bhatti, R. Qindeel, L. G. Bousiakou, N. Alonizan and A. Fazal e, Investigations of the structural, morphological and electrical properties of multilayer ZnO/TiO_2 thin films, deposited by sol–gel technique, *Results Phys.*, 2016, **6**, 156–160.

36 S. Chakma and V. S. Moholkar, Synthesis of bi-metallic oxides nanotubes for fast removal of dye using adsorption and sonocatalysis process, *J. Ind. Eng. Chem.*, 2016, **37**, 84–89.

37 D. M. King, X. Liang, Y. Zhou, C. S. Carney, L. F. Hakim, P. Li and A. W. Weimer, Atomic layer deposition of TiO_2 films on particles in a fluidized bed reactor, *Powder Technol.*, 2008, **183**, 356–363.

38 N. M. Bahadur, T. Furusawa, M. Sato, F. Kurayama and N. Suzuki, Rapid synthesis, characterization and optical properties of TiO_2 coated ZnO nanocomposite particles by a novel microwave irradiation method, *Mater. Res. Bull.*, 2010, **45**, 1383–1388.

39 M. A. Gondal, A. M. Ilyas and U. Baig, Pulsed laser ablation in liquid synthesis of ZnO/TiO_2 nanocomposite catalyst with enhanced photovoltaic and photocatalytic performance, *Ceram. Int.*, 2016, **42**, 13151–13160.

40 S. B. Galvão, A. C. Lima, S. N. de Medeiros, J. M. Soares and C. A. Paskocimas, The effect of the morphology on the magnetic properties of barium hexaferrite synthesized by Pechini method, *Mater. Lett.*, 2014, **115**, 38–41.

41 P. Wu, G. Wang, R. Chen, Y. Guo, X. Ma and D. Jiang, Enhanced visible light absorption and photocatalytic activity of $[KNbO_3]_{1-x}[BaNi_{0.5}Nb_{0.5}O_{3-[small\ delta]}]_x$ synthesized by sol–gel based Pechini method, *RSC Adv.*, 2016, **6**, 82409–82416.

42 M. Galceran, M. C. Pujol, M. Aguiló and F. Díaz, Sol–gel modified Pechini method for obtaining nanocrystalline $KRE(WO_4)_2$ (RE = Gd and Yb), *J. Sol-Gel Sci. Technol.*, 2007, **42**, 79–88.

43 H.-S. Lim, J. Lee, S. Lee, Y. S. Kang, Y.-K. Sun and K.-D. Suh, Walnut-like $ZnO@Zn_2TiO_4$ multicore–shell submicron spheres with a thin carbon layer: Fine synthesis, facile structural control and solar light photocatalytic application, *Acta Mater.*, 2017, **122**, 287–297.

44 P. J. Holliman, D. K. Muslem, E. W. Jones, A. Connell, M. L. Davies, C. Charbonneau, M. J. Carnie and D. A. Worsley, Low temperature sintering of binder-containing TiO_2/metal peroxide pastes for dye-sensitized solar cells, *J. Mater. Chem. A*, 2014, **2**, 11134–11143.

45 S. K. Talkhoncheh, M. Haghighi, S. Minaei, H. Ajamein and M. Abdollahifar, Synthesis of $CuO/ZnO/Al_2O_3/ZrO_2/CeO_2$ nanocatalysts *via* homogeneous precipitation and combustion methods used in methanol steam reforming for fuel cell grade hydrogen production, *RSC Adv.*, 2016, **6**, 57199–57209.

46 S. Janitabar-Darzi and A. R. Mahjoub, Investigation of phase transformations and photocatalytic properties of sol–gel prepared nanostructured ZnO/TiO_2 composites, *J. Alloys Compd.*, 2009, **486**, 805–808.

47 M. Zhu, S. Li, Z. Li, X. Lu and S. Zhang, Investigation of solid catalysts for glycolysis of polyethylene terephthalate, *Chem. Eng. J.*, 2012, **185–186**, 168–177.

48 R. Jenkins and R. L. Snyder, *Introduction to X-ray powder diffractometry*, John Wiley & Sons, Inc., New York, 1996.

49 J. Tian, J. Wang, J. Dai, X. Wang and Y. Yin, N-doped TiO_2/ZnO composite powder and its photocatalytic performance for degradation of methyl orange, *Surf. Coat. Technol.*, 2009, **204**, 723–730.

50 J. Arin, S. Thongtem, A. Phuruangrat and T. Thongtem, Characterization of $ZnO–TiO_2$ and zinc titanate nanoparticles synthesized by hydrothermal process, *Res. Chem. Intermed.*, 2016, 1–13.

51 Z. Mohammadi, S. Sharifnia and Y. Shavisi, Photocatalytic degradation of aqueous ammonia by using TiO_2ZnO/LECA hybrid photocatalyst, *Mater. Chem. Phys.*, 2016, **184**, 110–117.

52 L. Budigi, M. R. Nasina, K. Shaik and S. Amaravadi, Structural and optical properties of zinc titanates synthesized by precipitation method, *J. Chem. Sci.*, 2015, **127**, 509–518.

53 M. V. Nikolić, N. Obradović, K. M. Paraskevopoulos, T. T. Zorba, S. M. Savić and M. M. Ristić, Far infrared reflectance of sintered Zn_2TiO_4, *J. Mater. Sci.*, 2008, **43**, 5564–5568.

54 A. C. Chaves, S. J. G. Lima, R. C. M. U. Araújo, M. A. M. A. Maurera, E. Longo, P. S. Pizani, L. G. P. Simões, L. E. B. Soledade, A. G. Souza and I. M. G. d. Santos, Photoluminescence in disordered Zn_2TiO_4, *J. Solid State Chem.*, 2006, **179**, 985–992.

55 K. Nakamoto, *Infrared and Raman Spectra of Inorganic and Coordination Compounds, Applications in Coordination, Organometallic, and Bioinorganic Chemistry*, Wiley, 2009.

56 M. Y. Nassar, A. S. Attia, S. Adawy and M. F. El-Shahat, Novel isatinoxime molybdenum and chromium complexes: Synthesis, spectroscopic, and thermal characterization, *J. Mol. Struct.*, 2012, **1026**, 88–92.

57 M. Y. Nassar, A. S. Attia, K. A. Alfallous and M. F. El-Shahat, Synthesis of two novel dinuclear molybdenum(0) complexes of quinoxaline-2,3-dione: New precursors for preparation of α-MoO_3 nanoplates, *Inorg. Chim. Acta*, 2013, **405**, 362–367.

58 M. Mostafa, H. M. Saber, A. A. El-Sadek and M. Y. Nassar, Preparation and performance of $^{99}Mo/^{99m}Tc$ chromatographic column generator based on zirconium molybdosilicate, *Radiochim. Acta*, 2016, 257–265.

59 B. Golzad-Nonakaran and A. Habibi-Yangjeh, Photosensitization of ZnO with Ag_3VO_4 and AgI nanoparticles: Novel ternary visible-light-driven photocatalysts with highly enhanced activity, *Adv. Powder Technol.*, 2016, **27**, 1427–1437.

60 A. Akhundi and A. Habibi-Yangjeh, Novel magnetically separable $g\text{-}C_3N_4/AgBr/Fe_3O_4$ nanocomposites as visible-light-driven photocatalysts with highly enhanced activities, *Ceram. Int.*, 2015, **41**, 5634–5643.

61 Y. Xu and M. A. A. Schoonen, The absolute energy positions of conduction and valence bands of selected semiconducting minerals, *Am. Mineral.*, 2000, **85**, 543.

62 M. A. Butler and D. S. Ginley, Prediction of Flatband Potentials at Semiconductor–Electrolyte Interfaces from Atomic Electronegativities, *J. Electrochem. Soc.*, 1978, **125**, 228–232.

63 M. Shekofteh-Gohari and A. Habibi-Yangjeh, Ultrasonic-assisted preparation of novel ternary $ZnO/AgI/Fe_3O_4$ nanocomposites as magnetically separable visible-light-driven photocatalysts with excellent activity, *J. Colloid Interface Sci.*, 2016, **461**, 144–153.

64 K. Sarkar, E. V. Braden, T. Froschl, N. Husing and P. Muller-Buschbaum, Spray-deposited zinc titanate films obtained *via* sol–gel synthesis for application in dye-sensitized solar cells, *J. Mater. Chem. A*, 2014, **2**, 15008–15014.

65 I. Velo-Gala, J. J. López-Peñalver, M. Sánchez-Polo and J. Rivera-Utrilla, Activated carbon as photocatalyst of reactions in aqueous phase, *Appl. Catal., B*, 2013, **142–143**, 694–704.

66 J. Zhang and Z. Ma, Novel [small beta]-$Ag_2MoO_4/g\text{-}C_3N_4$ heterojunction catalysts with highly enhanced visible-light-driven photocatalytic activity, *RSC Adv.*, 2017, **7**, 2163–2171.